Frequency-domain magnetic-resonance spectroscopic investigations of the magnetization dynamics in $Mn_{12}Ac$ single crystals

J. van Slageren,[1,2,*] S. Vongtragool,[1] B. Gorshunov,[3] A. Mukhin,[3] and M. Dressel[1]
[1]*1. Physikalisches Institut, Universität Stuttgart, Pfaffenwaldring 57, 70550 Stuttgart, Germany*
[2]*School of Chemistry, University of Nottingham, Nottingham NG7 2RD, United Kingdom*
[3]*Prokhorov General Physics Institute, Russian Academy of Sciences, Moscow, Russia*
(Received 18 July 2008; revised manuscript received 27 April 2009; published 5 June 2009)

A comprehensive spectroscopic study of the magnetization relaxation of $Mn_{12}Ac$ is presented. The single crystalline samples are investigated as a function of magnetic field and temperature using frequency-domain magnetic-resonance spectroscopy. The magnetization relaxation is followed in real-time by recording spectra as a function of delay time. The experiments are performed both in the absence of a magnetic field and in external fields either parallel (Faraday geometry) or perpendicular (Voigt geometry) to the direction of radiation. The relaxation rates obtained from spectral fits correspond well to those obtained from magnetometric measurements. The results exhibit clear signatures of quantum tunneling of the magnetization. The influence of D strain and internal dipolar fields is observed.

DOI: 10.1103/PhysRevB.79.224406 PACS number(s): 75.50.Xx, 75.20.−g, 76.30.Fc, 33.35.+r

I. INTRODUCTION

The magnetic properties of single-molecule magnets (SMMs) have been the subject of many, extremely detailed, experimental and theoretical investigations.[1,2] This interest initially arose because of the discovery that these molecules show magnetic hysteresis in the absence of magnetic ordering. In subsequent years, it was discovered that SMMs show both classical and quantum phenomena, which attracted much additional attention. They are unique objects to study physical phenomena, such as molecular magnetic bistability, quantum tunneling of magnetization, quantum phase interference, and quantum coherence on the mesoscopic scale (i.e., between quantum microscopic and classical macroscopic scales).[3–8] A large variety of SMMs have been prepared with the number of ions ranging from 2 to 84.[9,10] In spite of this large range of available SMMs, by far most studies have been performed on a dodecanuclear manganese cluster $[Mn_{12}O_{12}(CH_3COO)_{16}(H_2O)_4]\cdot 2CH_3COOH\cdot 4H_2O$,[11] abbreviated as $Mn_{12}Ac$, which has a ground-state spin of $S=10$.

The reason that SMMs lend themselves well to such detailed studies is that they are absolutely monodisperse, i.e., in a macroscopic crystal all molecules are exactly the same. The fascinating physical properties of SMMs originate from the interplay between the exchange interaction between the paramagnetic ions that compose the cluster, the zero-field splitting (ZFS) of these ions and the external magnetic field. In most studies, only the spin ground state is considered (giant spin approximation), although it was recently shown that this approximation is not always valid.[12–15] One subject that has received particular attention is that of the magnetization relaxation. The collective effect of the axial single-ion anisotropies (zero-field splittings) stabilizes the magnetic moment of the cluster along the molecular easy axis, in other words it stabilizes the $M_S=\pm S$ states. This creates an energy barrier for inversion of the magnetic moment, leading to magnetic hysteresis, if the thermal energy is small compared to this energy barrier.

In addition, the magnetic moment can tunnel under the barrier, which has been named quantum tunneling of the magnetization (QTM).[1] The observation of a hybrid magnetization relaxation process called thermally assisted quantum tunneling, in which the system is thermally excited to higher M_S levels, followed by QTM underlines the mesoscopic nature of SMMs. QTM is only possible if two M_S levels on both sides of the energy barrier are in resonance, which occurs at distinct longitudinal field values leading to pronounced minima in the relaxation time as a function of the field.[1,3,4] At $T=0$, thermal relaxation and thermally assisted tunneling are no longer possible, and quantum tunneling of the magnetization is the only relaxation pathway. QTM also requires that an interaction exists that mixes these two levels. It is usually assumed that the transverse zero-field splitting is the main responsible interaction. The origin of second-order transverse ZFS is the collective effect of the single-ion anisotropies, while fourth-order anisotropy is currently thought to arise mainly from mixing between the spin ground state and spin-excited states of the cluster.[12,13,16] An appropriate spin Hamiltonian to describe the spin ground state is

$$\mathcal{H} = D\hat{S}_z^2 + B\hat{S}_z^4 + 2E(\hat{S}_+^2 + \hat{S}_-^2) + \frac{1}{2}C(\hat{S}_+^4 + \hat{S}_-^4) + g\mu_B\hat{\mathbf{S}}\cdot\mathbf{H}. \tag{1}$$

In this equation, the first two terms are the second- and fourth-order axial ZFS, the second two terms are the second- and fourth-order transverse ZFS, while the last term is the Zeeman interaction with an effective magnetic field $\mathbf{H}$. $\hat{S}_z$ is the z-component of the spin operator $\hat{\mathbf{S}}$, while $\hat{S}_+$ and $\hat{S}_-$ are the raising and lowering operators, respectively: $\hat{S}_\pm = \hat{S}_x \pm i\hat{S}_y$. The parameters D, B, E, and C are the magnetic anisotropy constants, and g is the isotropic g factor. The large energy barrier of approximately 65 K, caused by the axial ZFS, sets the energy scale in $Mn_{12}Ac$.

The transverse interactions of this spin Hamiltonian cannot mix *any* two M_S levels. The E term can mix two M_S levels with $\Delta M_S=2n$ with n an integer, while the C term can mix two M_S levels with $\Delta M_S=4n$. In $Mn_{12}Ac$ one would

therefore only expect quantum tunneling at odd-to-odd and even-to-even M_S crossings. In addition, $Mn_{12}Ac$ has almost tetragonal symmetry, which precludes the presence of a nonzero E term, and therefore quantum tunneling is limited to even-to-even M_S crossings. Although in $Mn_{12}Ac$ this symmetry is decreased due to local disorder,[17,18] recently published measurements evidence that quantum tunneling does occur at odd-to-odd transitions in a different Mn_{12} derivative (Mn_{12}tBuAc) with crystallographic axial symmetry and which was reported to have less disorder.[19]

In none of these cases should quantum tunneling occur at odd-to-even and even-to-odd M_S crossings. In spite of a decade of intense investigation, it is unclear what interaction relaxes the expected tunneling selection rules. A possible reason lies in the transverse fields caused by tilting of the molecular easy axis in $Mn_{12}Ac$ due to disorder,[20] but this seems to be ruled out as a general cause by the fact that quantum tunneling does occur at odd-to-odd transitions in Mn_{12}tBuAc which has no disorder. Second, it has been shown theoretically that the nonlinear effect of the combination of the zero-field splitting and intermolecular transverse magnetic-dipolar interaction can produce the observed absence of tunneling selection rules.[21] Mn_{12}tBuAc has twice the unit cell volume compared to the former, which decreases but not precludes transverse magnetic-dipolar interactions. A third possible origin is the occurrence of antisymmetric exchange, which has been proposed to occur in Mn_{12} and in Ni_4 clusters.[14,22]

The majority of the experimental studies on the magnetization dynamics in Mn_{12} were performed with magnetometric techniques.[3,4,19,23–28] These techniques measure only the total magnetization or susceptibility of the sample. Much more information may be gained using spectroscopic methods because they are microscopic probes of the sample properties. Spectroscopic methods can for instance distinguish between different species in the sample, in the case of Mn_{12} the normal- and fast-relaxing species. Spectroscopic methods can also yield more detailed information than magnetometric methods because they couple to a specific property of the material, e.g., the nuclear or the electronic spins. Thus, it was shown experimentally by NMR spectroscopy that the nuclear-spin relaxation in $Mn_{12}Ac$ is intricately linked with the electronic spin tunneling.[29]

The electronic spin can be addressed with several different experimental methods. As an example, it was recently demonstrated that the magnetization dynamics in $Mn_{12}Ac$ can be followed using inelastic neutron spectroscopy (INS).[30] Although very elegant, these measurements suffered from the lack of sensitivity of the INS technique, which precluded measurements in real time. In addition, the resolution in INS is rather limited.

A technique that does not suffer from these disadvantages is electron-spin resonance (ESR). High-frequency ESR measurements have been essential in determining the transverse spin-Hamiltonian parameters as well as for the study of dipolar interactions in $Mn_{12}Ac$ and other single-molecule magnets.[31,32] Recently, a preliminary study of the magnetization relaxation in $Mn_{12}Ac$ by ESR was published.[33] However, for the study of magnetization relaxation and quantum tunneling of the magnetization, it is convenient to measure the magnetic-resonance spectra in the frequency domain rather than the field domain because the magnetization relaxation rate is field dependent, but not frequency dependent. In recent years, we have extensively used the technique of frequency-domain magnetic-resonance spectroscopy (FDMRS) for the study of single-molecule magnets.[15,34–40] In this technique it is the frequency that is swept, rather than the external magnetic field. This property makes the technique excellently suited for the spectroscopic study of the magnetization dynamics in single-molecule magnets. The experiments are performed either without magnetic field or in the presence of an external field. In this study, we were particularly interested in the influence of dipolar interactions and D strain on the magnetization dynamics.

For our investigations we have chosen the well-known $Mn_{12}Ac$ system because the crystals can be aligned by eye, the magnetization relaxation behavior can be studied at ^{4}He temperatures, and the spin-Hamiltonian parameters are well known. The magnetization decay is exponential at longer delay times, but faster at short delay times.[41] The fast short-time-delay magnetization relaxation, which persists in dilute solution,[42] was attributed to hyperfine and/or dipolar-interaction-induced tunneling, which leads to the magnetization decaying with the square root of time.[41,43,44]

Here we present a detailed and comprehensive study of the magnetization relaxation in $Mn_{12}Ac$ single-crystal mosaics. First of all, we show the results of measurements that serve to compare the properties of the present single-crystal mosaics to those of microcrystalline samples we have studied previously (Sec. IV A). In the second part we discuss in detail the in-field relaxation studies performed in Voigt geometry (Sec. IV B), which includes the spectroscopic study of quantum tunneling of the magnetization. Finally, in Sec. IV C we present the results of relaxation measurements in Faraday geometry both in the presence and absence of a magnetic field. The main findings of these studies are that we can measure the magnetization relaxation by magnetic-resonance methods which enable the direct observation of the population of different levels. Second, we can observe quantum tunneling of the magnetization. Finally, we see the influence of D strain and internal dipolar fields in the magnetic-resonance spectra.

II. EXPERIMENTAL PROCEDURES

Crystals of $Mn_{12}Ac$ of approximate $1\times1\times3$ mm^3 size were prepared by literature methods.[11] The longest axis of the crystal corresponds to the crystallographic c axis. The crystal size precludes measurements on a single crystal. First of all, the sensitivity of the FDMRS method is not sufficient for such small samples. Second, in the measurement setup, an aperture is located just in front of the sample, to ensure that all detected radiation passed through the sample. The size of the sample therefore determines the size of the aperture. This in turn limits the lowest frequency that can be employed, as radiation with a wavelength longer than the size of the aperture is not transmitted through the aperture.[45] For distortion-free spectra the aperture should be larger than two to three times the wavelength of the radiation. For the smallest dimension of the single crystals employed (ca. 1

mm), that would mean a lowest frequency of 20 cm^{-1} (λ =0.5 mm), which is clearly above the frequency region where magnetic-resonance transitions can be expected (around 10 cm^{-1}). Therefore, we have resorted to preparing single-crystal mosaics of around 20 single crystals. These crystals were glued to a small piece of thin mylar foil, with their c axes aligned parallel to each other. The resulting mosaic was very carefully polished to give two plane parallel faces, which greatly improved the quality of the spectra. Two different samples were prepared. In the first the crystals were mounted with their c axes parallel to the plane of the sample, while in the second the c axes were oriented perpendicular to that plane. These samples will be denoted sample V and sample F below. The thickness of both samples was approximately 0.5 mm. We estimate that the single crystals were coaligned with an accuracy better than 3°.

All experiments were performed using frequency-domain magnetic-resonance spectroscopy. The spectrometer is a quasioptical transmission setup which employs backward-wave oscillators (BWO) as coherent sources of linearly polarized terahertz radiation (millimeter and submillimeter wavelength), and a Golay cell as detector [Fig. 1(a)].[34,46] The sample is inserted into an Oxford Instruments Spectromag 4000 split-coil optical magnet (T=1.7–300 K, H=0–8 T). The magnetic field **H** can be aligned parallel to the radiation propagation direction **q** (Faraday geometry) or perpendicular to it (Voigt geometry). Both measurement geometries were utilized in this study. In Faraday geometry, the oscillating magnetic field **h** of the electromagnetic radiation is necessarily perpendicular to the external magnetic field ($\mathbf{h} \perp \mathbf{H}$), but in Voigt geometry $\mathbf{h} \perp \mathbf{H}$ or $\mathbf{h} \| \mathbf{H}$. These two orientations of the radiation magnetic field with respect to the external field correspond to perpendicular and parallel mode ESR, respectively, and are obtained by using wire-grid polarizers that linearly polarize the radiation in the desired direction.

In all experiments, the external field **H** was applied parallel to the c axis of the crystal which corresponds to the easy axis of the molecules. Therefore for measurements in Voigt geometry sample V was used, while sample F was employed for Faraday geometry measurements.

The time-resolved measurements of Secs. IV B and IV C were performed in the following manner:

(1) The sample was field cooled in a positive magnetic field $+H$. At the employed low temperatures ($T \lesssim 2$ K) the only significant population is in the $|+10\rangle$ M_S state [Fig. 1(b)].

(2) Once the temperature stability was better than 0.005 K, the field was inverted to $-H$ at maximum field sweep rate ($\sim$1 T/min). At this point the sample is in the metastable $|+10\rangle$ state and will start to relax to the $|-10\rangle$ state [Fig. 1(c)].

(3) After field inversion, transmission spectra were recorded as a function of time. The data acquisition takes approximately 20 s per scan. During this time the sample relaxes and hence the resonance line due to the transition from the metastable state $|+10\rangle \rightarrow |+9\rangle$ transition will disappear while that due to the transition from the ground state $|-10\rangle \rightarrow |-9\rangle$ will appear.

The zero-field relaxation experiments on sample F were performed in a similar manner, but the field was switched off rather than inverted after field cooling. In virtually all experiments the radiation magnetic field was linearly polarized perpendicular to the crystal c axis.

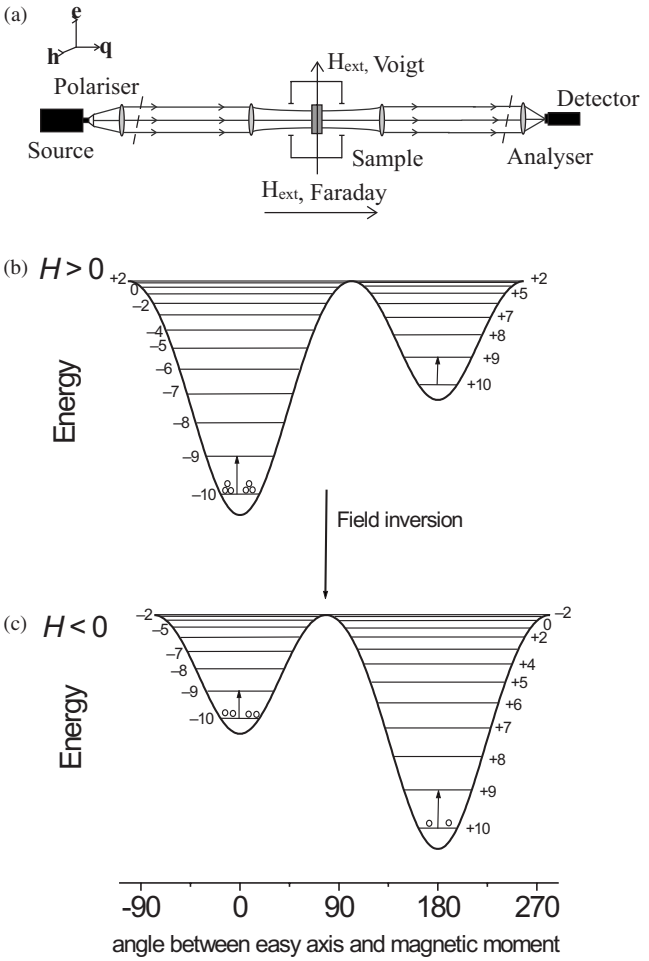

FIG. 1. (a) Schematic spectrometer setup showing the directions of the external magnetic field **H**, the radiation propagation direction **q**, and the magnetic field direction of the terahertz radiation **h**. In Faraday geometry $\mathbf{h} \perp \mathbf{H}$, while in Voigt geometry $\mathbf{h} \perp \mathbf{H}$ or $\mathbf{h} \| \mathbf{H}$. (b) Energy levels in the presence of an external magnetic field $H > 0$. (c) Arrangement of the energy levels after inversion of the magnetic field.

III. THEORETICAL MODELING

FDMRS spectra are recorded in transmission as a function of frequency. The transmission is determined by the two complex optical parameters which are the magnetic permeability ($\mu^* = \mu' + i\mu''$) and the dielectric permittivity ($\epsilon^* = \epsilon' + i\epsilon''$), which in general are tensorial quantities (see below). In FDMRS spectra, the magnetic-dipole transitions lead to a frequency dispersion of the magnetic permeability determined by the line-shape function, R, the resonance frequency, ν_{res}, and the mode contribution to the permeability (resonance intensity), $\Delta\mu$.[46,47] The resonance frequencies can be extracted from the energy levels obtained from the Hamiltonian [Eq. (1)]. For the simulation of our spectra we employed the following spin-Hamiltonian parameters: $D = -0.389$ cm^{-1}, $B = -7.65 \times 10^{-4}$ cm^{-1}, and $g = 1.94$. For

all simulations, we used the Gaussian line-shape function, which is a complex function consisting of the real (R') and imaginary (R'') parts,

$$R_k'' = \sqrt{\frac{\pi}{8}}\frac{\nu}{\sigma_k}\left\{\exp\left[-\frac{(\nu-\nu_k)^2}{2\sigma_k^2}\right]+\exp\left[-\frac{(\nu+\nu_k)^2}{2\sigma_k^2}\right]\right\}, \tag{2a}$$

and

$$R_k'(\nu) = \frac{2}{\pi}\int_0^\infty \frac{\nu_1 R_k''(\nu_1)}{\nu_1^2-\nu^2}\mathrm{d}\nu_1, \tag{2b}$$

where σ_k is the Gaussian linewidth, which corresponds to a full width at half maximum FWHM$=2\sqrt{2\ln 2}\sigma_k$). The mode contributions to the x and y components of the permeability (intensity) of the magnetic-resonance transition between levels i and f are given by

$$\Delta\mu_{if} \equiv \Delta\mu_{if}^{xx,yy} = 8\pi N g^2 \mu_B^2 \frac{|\langle f|S_{x,y}|i\rangle|^2}{h\nu_{if}}\frac{\rho_i-\rho_f}{Z}, \tag{3}$$

where N is the density of molecules, Z is the partition function, and ρ_i and ρ_f are the populations of initial and final states. In the nonmagnetized state, the magnetic permeability of $Mn_{12}Ac$ is given by its x and y components ($\mu_{xx}=\mu_{yy}\equiv\mu$) which are given by

$$\mu = 1+\sum_{if}\Delta\mu_{if}R_{if}, \tag{4}$$

and from that together with the dielectric permittivity the transmission Tr for the $h\perp z$ polarization can be calculated by using the Fresnel formulas,[48]

$$\mathrm{Tr}(\nu) = E\frac{(1-R)^2+4R\sin^2\psi}{(1-RE)^2+4RE\sin^2(N+\psi)}, \tag{5}$$

where

$$E=\exp\left(\frac{-4\pi kd}{\lambda}\right),\quad R=\frac{(a-1)^2+b^2}{(a+1)^2+b^2},$$

$$N=\frac{2\pi nd}{\lambda},\quad \psi=\arctan\left(\frac{2b}{a^2+b^2-1}\right),$$

$$n+ik=\sqrt{\epsilon\mu},\quad a+ib=\sqrt{\frac{\mu}{\epsilon}}.$$

In this study, two additional factors are important. First of all, the resonance-line intensities depend on the time-dependent populations $\rho_{\pm 10}$ of the ground ($|+10\rangle$) and metastable ($|-10\rangle$) M_S states, which gives for the $|+10\rangle\rightarrow|+9\rangle$ and for the $|-10\rangle\rightarrow|-9\rangle$ transitions

$$\Delta\mu_{+10} = \rho_{+10}\Delta\mu_0\frac{\nu_0}{\nu_{+10}},$$

$$\Delta\mu_{-10} = \rho_{-10}\Delta\mu_0\frac{\nu_0}{\nu_{-10}}. \tag{6}$$

Here $\rho_{\pm 10}$ are the populations of the $|\pm 10\rangle$ states with $\rho_{+10}+\rho_{-10}=1$ (the populations of the excited $|\pm 9\rangle$ states are neglected at low temperatures), and $\Delta\mu_0$ and ν_0 are the mode contribution (resonance-line intensity) and resonance frequency, respectively, for nonmagnetized samples in zero applied field.

Second, in magnetized samples, (i.e., in a gyrotropic medium), the magnetic-permeability tensor contains also nondiagonal components which leads to different effective magnetic permeabilities depending on the relative orientations of magnetization and radiation propagation direction.[36,39,49] The magnetic-permeability tensor is[49]

$$\mu = \mu_0\begin{pmatrix}\mu & i\kappa & 0\\ -i\kappa & \mu & 0\\ 0 & 0 & 1\end{pmatrix}, \tag{7}$$

where the tensor elements contain the sum over all the magnetic-resonance mode contributions to the magnetic permeabilities [Eq. (4)], which in the present case are just the $|+10\rangle\rightarrow|+9\rangle$ and $|-10\rangle\rightarrow|-9\rangle$ transitions

$$\mu = 1+\sum_i \Delta\mu_i R_i(\nu) = 1+\Delta\mu_{+10}R_{+10}+\Delta\mu_{-10}R_{-10},$$

$$\kappa = \sum\frac{\nu}{\nu_i}\Delta\mu_i R_i(\nu) = \frac{\nu}{\nu_{+10}}\Delta\mu_{+10}R_{+10}-\frac{\nu}{\nu_{-10}}\Delta\mu_{-10}R_{-10}. \tag{8}$$

The electromagnetic wave propagation in magnetized media is different from longitudinally magnetized media (Faraday geometry) and transversely magnetized media (Voigt geometry), leading to different effective magnetic permeabilities μ_{eff} in both cases.[49] In Voigt geometry, for contributions of the two abovementioned resonance modes, the effective magnetic permeability is

$$\mu_{\mathrm{eff}}^{\mathrm{V}} = \frac{\mu^2-\kappa^2}{\mu} \approx 1+\frac{\Delta\mu_{+10}R_{+10}(\nu)+\Delta\mu_{-10}R_{-10}(\nu)}{1+\Delta\mu_{+10}R_{+10}(\nu)+\Delta\mu_{-10}R_{-10}(\nu)}. \tag{9}$$

In this derivation, the factors $\nu/\nu_{\pm 10}$ that appear in κ have been approximated as 1 over the frequency range considered. As we have shown previously,[36] this change in magnetic permeability going from a nonmagnetized to a magnetized medium leads to a shift in the apparent resonance-line position, without a change in resonance frequency. This is easiest to see for a Lorentzian line-shape function $R(\nu)=\nu_{\mathrm{res}}^2/(\nu_{\mathrm{res}}^2-\nu^2)$. For a fully magnetized sample ($\rho_{+10}\approx 1, \rho_{-10}\approx 0$), and a Lorentzian line shape, the denominator in Eq. (9) simplifies to $1+\Delta\mu_{+10}\nu_{\mathrm{res}}^2/(\nu_{\mathrm{res}}^2-\nu^2)$. The apparent resonance-line position is where this denominator goes to zero, i.e., at $\nu=\nu_{+10}\sqrt{\Delta\mu+1}$.

In Faraday geometry, it is convenient to separate the linear polarization into its two circularly polarized components (left-handed, LH, and right-handed, RH). The LH component only excites $\Delta M_S=-1$ and the RH component only ΔM_S

=+1 transitions.[50] The effective magnetic permeability is $\mu_{\text{eff}}^{\text{F}}=\mu\pm\kappa$, where the plus sign is valid for the RH component, or more specifically in the present case,

$$\mu_{\text{eff}}^{\text{F,LH}} \approx 1 + 2\Delta\mu_{+10}R_{+10},$$

$$\mu_{\text{eff}}^{\text{F,RH}} \approx 1 + 2\Delta\mu_{-10}R_{-10}. \quad (10)$$

The resonance-line intensities ($\Delta\mu$) and Gaussian linewidths (σ) were extracted from the spectra recorded before inversion of the field. The resonance frequencies were obtained from the Hamiltonian [Eq. (1)], where the effective magnetic field in the Zeeman term was corrected for the internal dipolar field which depends on the net magnetization of the sample,

$$H_{\text{eff}} = H_{\text{applied}} + H_{\text{dip}}(\rho_{+10} - \rho_{-10}). \quad (11)$$

The spectra were then fitted, where the only fit parameters were the populations $\rho_{\pm 10}$. An exponential function was fitted to the populations as a function of time, yielding the relaxation time. Because we fit a significant proportion (usually all) of the complete magnetization decay, we are not concerned with the particularities of short delay relaxation rates. We found monoexponential behavior in all cases and there was no need to introduce stretched exponential functions, which were invoked in the past.[1]

The relaxation times in Sec. IV B were calculated on a basis of the theory developed for the description of the magnetization relaxation in $Mn_{12}Ac$ which takes into account phonon-assisted spin tunneling induced by the fourth-order transverse zero-field splitting and an effective transverse magnetic field.[21,51–53] The numerical diagonalization of the master equation for the density matrix of $Mn_{12}Ac$ was performed in the space of the ground $S=10$ multiplet following reported procedures.[54] We have taken as the speed of sound $c=1.75\times10^3$ m/s, the density $\rho=1.83$ g/cm^{-3} in addition to reported zero-field splitting parameters of $Mn_{12}Ac$.[53]

IV. RESULTS AND DISCUSSION

A. Static measurements

1. Zero magnetic field

The transmission spectra displayed in Fig. 2 were recorded on sample V between 6 and 12 cm^{-1} with different polarization of the radiation: $\mathbf{h}\|\mathbf{c}$ and $\mathbf{h}\perp\mathbf{c}$. The spectra show a pronounced oscillation in the baseline, while only in those for $\mathbf{h}\perp\mathbf{c}$ [Fig. 2(b)] two clear magnetic-resonance lines are observed. The oscillation is due to Fabry-Pérot-type interference within the plane parallel sample.[34,46] The depth and period of the oscillations are exclusively determined by the dielectric permittivity and the thickness of the sample. A fit of both spectra using the Fresnel formulas (disregarding the magnetic-resonance lines) evidences that the dielectric permittivity is anisotropic, with the real parts $\epsilon'_{\|}=5.1\pm1.5$ (electric field vector of the radiation $\mathbf{e}\|\mathbf{c}$), and $\epsilon'_{\perp}=6.4\pm1.0$ ($\mathbf{e}\perp\mathbf{c}$); the imaginary parts equal to zero. The magnetic-resonance lines are absent for $\mathbf{h}\|\mathbf{c}$ because an oscillating magnetic field parallel to the molecular quantization axis cannot induce magnetic-resonance transitions. This is in agreement with the well-known observation in electron-spin-resonance spectroscopy that magnetic-resonance lines are only detected if $\mathbf{h}\perp\mathbf{H}$ (perpendicular mode ESR), and not if $\mathbf{h}\|\mathbf{H}$ (parallel mode ESR), where $\mathbf{H}$ is the external magnetic field.[50] In the single-crystal $Mn_{12}Ac$ samples under study, the quantization axis is given by the ZFS unique c-axis rather than the external magnetic field. The high- and low-frequency magnetic-resonance lines are attributed to the $|\pm10\rangle\rightarrow|\pm9\rangle$ and $|\pm9\rangle\rightarrow|\pm8\rangle$ transitions, respectively.[55] These results demonstrate that our samples are indeed single-crystalline and that the c axes of the crystals are well oriented parallel to each other. The resonance frequencies are exactly the same as those observed for pressed powder pellets of Mn_{12},[55] and the spin-Hamiltonian parameters are therefore unchanged.

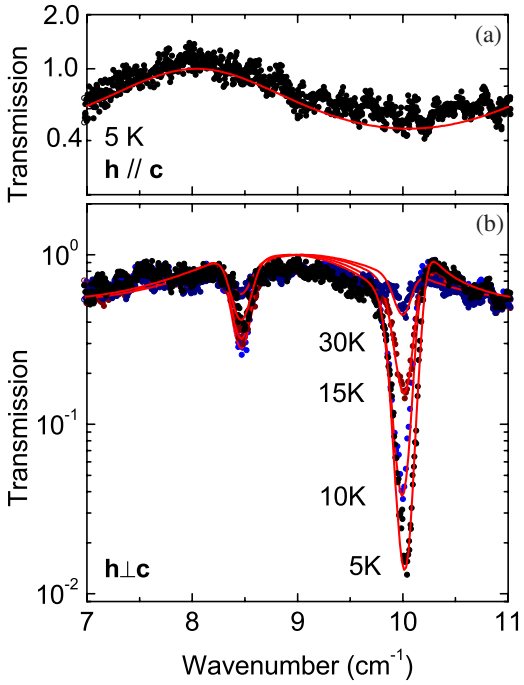

FIG. 2. (Color online) Zero-field FDMRS spectra recorded on sample V of $Mn_{12}Ac$ at (a) $T=5$ K and $\mathbf{h}\|\mathbf{c}$, and (b) for various temperatures and $\mathbf{h}\perp\mathbf{c}$, with the crystal c axes in the plane of the 0.49 mm thick sample.

In previous studies we found that the resonance lines can be simulated better by using a Gaussian line-shape function than by using a Lorentzian line.[36,56] This indicates that the linewidth is governed by distributions in the sample, including those in the ZFS D parameter (D strain), magnetodipolar interactions, and hyperfine interactions, rather than by the excited-state lifetime. From the simulations in the present study we found a linewidth of $\sigma=(0.085\pm0.05)$ cm^{-1}. We have previously shown that mainly the distribution in D parameters contributes to the observed linewidth, where in $Mn_{12}Ac$ this distribution consists of a discrete set of isomers rather than a continuous Gaussian distribution,[36] in agreement with EPR measurements reported in literature.[20] However, we felt that the data quality does not enable us to follow the magnetization dynamics of the separate isomers, and have therefore assumed a Gaussian line shape in the analysis.

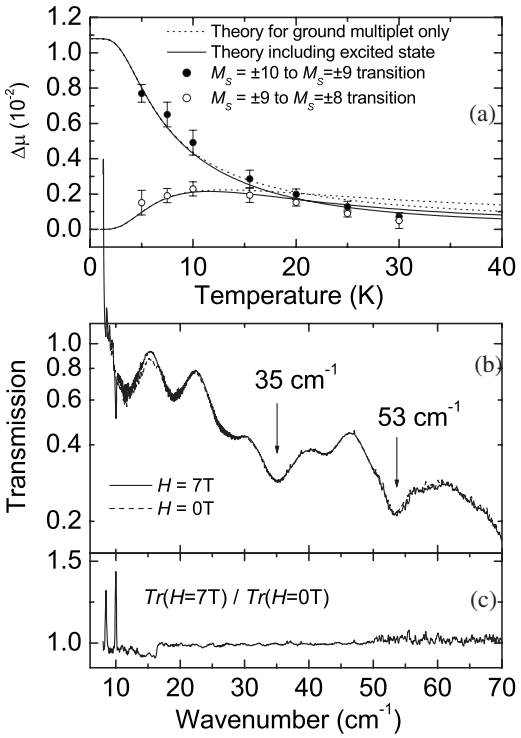

FIG. 3. (a) Temperature dependence of the resonance-line intensities $\Delta\mu$ obtained from the fits of the transmission spectra for the $|\pm 10\rangle \rightarrow |\pm 9\rangle$ and $|\pm 9\rangle \rightarrow |\pm 8\rangle$ transitions. The lines correspond to theoretically predicted temperature dependences of $\Delta\mu$ taken into account the ground-state multiplet only (dotted lines) or excited states, too (solid line). (b) Far-infrared transmission spectra recorded on a pressed powder pellet of $Mn_{12}Ac$ at $H=0$ and $H=7$ T. Two magnetic-resonance lines are observed at low frequencies and two optical phonon transitions at 35 and 53 cm^{-1}, respectively. Panel C shows the ratio of the transmission spectra: Tr($H=7$ T) divided by the zero-field data.

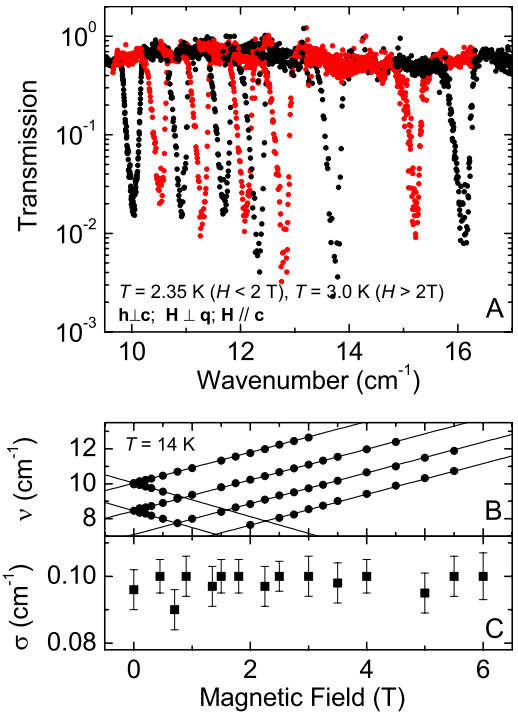

FIG. 4. (Color online) (a) FDMRS spectra of $Mn_{12}Ac$ recorded at on (field-cooled) sample V for different static magnetic fields $\mathbf{H}\|\mathbf{c}$, where the temperature was $T=2.35$ K ($H<2$ T) and 3.0 K ($H\geq 2$ T). The magnetic absorption line shifts monotonously to higher frequencies as the applied field $\mathbf{H}$ increases. The field strength applied is (from left to right): 0, 0.45, 0.90, 1.35, 1.80, 2.25, 2.50, 3.00, 4.00, 6.00, and 7.00 T). (b) Resonance frequencies as a function of external magnetic field ($\mathbf{H}\|\mathbf{c}$) obtained from measurements on sample V at $T=14$ K (symbols). The drawn lines were calculated according to $\nu_{\mathrm{res}}=\nu_0+g_z\mu_B H_z$ with $g=1.94$. (c) Gaussian linewidth as a function of magnetic field.

Both resonance frequency and linewidth are temperature independent, but the intensity strongly depends on temperature due to the Boltzmann populations of the M_S states involved. Figure 3 displays the resonance-line intensities $\Delta\mu$ obtained from the fits of the spectra as a function of temperature, as well as the theoretically expected temperature dependence calculated considering the ground spin multiplet only (dotted line). At low temperatures the experimental and theoretical intensities match well. However, at higher temperatures, the experimental intensities are clearly lower than those calculated. Inclusion of an excited state at 40 cm^{-1} in the partition function of the Boltzmann distribution calculation yields a marked improvement in the calculated values [Fig. 3(a), solid lines].

Far-infrared measurements [Fig. 3(b)], exhibit an excitation at 35–40 cm^{-1}. The absence of magnetic field dependence indicates its nonmagnetic origin, and we therefore assign it to an optical phonon excitation.[57] Such an excitation is not expected to influence the magnetic-resonance spectrum in the absence of strong spin-phonon coupling. However, inelastic neutron-scattering measurements exhibit a double-peak excitation with maxima at 43 and 50 cm^{-1}, which was attributed to the transition from the $M_S=\pm 10$ level of the $S=10$ ground multiplet to the $M_S=\pm 9$ level of an $S=9$ excited state.[58,59] This intermultiplet transition is forbidden in magnetic-resonance spectroscopy, but the position of the $S=9$ excited state at about 40 cm^{-1} was inferred from the temperature dependence of magnetic-resonance lines that were assigned to transitions within this excited multiplet in EPR studies of $Mn_{12}tBuAc$.[60] The temperature dependence of the FDMRS intensities as displayed in Fig. 3(b) confirms the presence of a low-lying excited spin state.

2. Finite magnetic field

To investigate the possible presence of a distribution in g values (g strain) and in preparation for our studies of the magnetization dynamics (see below), we recorded FDMRS spectra at different fields applied along the easy axis ($\mathbf{H}\|\mathbf{c}$) at $T=2.35$ K [Fig. 4(a)]. The only resonance line visible is that due to the $|\pm 10\rangle \rightarrow |\pm 9\rangle$ transition at 10.0 cm^{-1} in zero field. The position of the resonance line $\tilde{\nu}_{\mathrm{res}}$ depends linearly on the external magnetic field, due to the Zeeman interaction, as displayed in Fig. 4(b) for measurements at $T=14$ K. A fit to $\tilde{\nu}_{\mathrm{res}}=\tilde{\nu}_0+g_z\mu_B H_z$ yields the g value $g_z=1.94\pm 0.01$ in good agreement with the value obtained by Barra *et al.* ($g_z=1.93\pm 0.01$).[61] Other reported g values are

g_z=1.97–2.08,[62] and g=2.0.[30] At T=14 K, the Gaussian linewidth is field-independent within our experimental error, which indicates that g strain is not a significant line-broadening factor in our case. The accurate measurements by Hill and collaborators revealed a g strain of the order of $\sigma_g = 0.002g$.[31,63] The resonance lines are all asymmetric (with the exception of that recorded in zero field), which is due to a combination of the fact that the medium is magnetized (field-cooled) and that the line shape is Gaussian.[36] In magnetized media, the macroscopic magnetic permeability and dielectric permittivity are represented by 3×3 tensors with nonzero off-diagonal elements in the directions perpendicular to the radiation propagation. These off-diagonal elements are ultimately responsible for effects such as Faraday rotation. The magnetic-resonance phenomenon influences only the magnetic permeability but not the dielectric properties. Importantly, the effective magnetic permeability obtained from the magnetic-permeability tensor (see Sec. III) is very different for media that are magnetized perpendicular to the radiation propagation direction (transversely magnetized media) compared to media that are magnetized along the radiation propagation direction (longitudinally magnetized media). While in the former case resonance lines become asymmetric and shift slightly,[36] in the latter case huge rotations of the plane of polarization are caused by the Faraday effect, which we observed in Mn_{12}Ac (see Sec. III).[39]

In the following section we turn to the investigation of the magnetization dynamics studied by FDMRS, first in Voigt geometry (Sec. IV B), then in Faraday geometry (Sec. IV C).

B. Relaxation measurements in Voigt geometry

Figure 5 displays an example of the investigation of the magnetization relaxation of Mn_{12}Ac by FDMRS. The sample is cooled down to T=1.75 K in an external field of H_z= +1.85 T [Fig. 1(b)]. At this point just the $|-10\rangle$ state is occupied, and the absorption line due to the $|-10\rangle \rightarrow |-9\rangle$ transition is observed at 11.78 cm^{-1} [the spectrum labeled "∞" in Fig. 5(a)]. Then the magnetic field is reversed to H_z= −1.85 T, which takes about 3 min, after which the $|-10\rangle$ state is metastable [Fig. 1(c)]. After inverting the magnetic field, the resonance line due to the $|-10\rangle \rightarrow |-9\rangle$ transition is at the much lower frequency of 8.45 cm^{-1} [the spectrum labeled "3" in Fig. 5(b)]. No resonance line is observed at 11.78 cm^{-1} immediately after field inversion [the spectrum labeled "1" in Fig. 5(a)]. As time elapses, a resonance line grows, which is attributed to the $|+10\rangle \rightarrow |+9\rangle$ transition [Fig. 1(c)]. Correspondingly the absorption line due to the $|-10\rangle \rightarrow |-9\rangle$ transition disappears over time, in agreement with the depopulation of the metastable state. It can be clearly noticed that the positions of the absorption lines shift in frequency (by up to 0.2 cm^{-1}) during the relaxation process. In addition, the line shape changes.[36] This can be explained as the combined effect of the change in internal magnetodipolar field and the off-diagonal elements in the magnetic-permeability tensor,[36] and will be discussed in more detail below. It should be noted that in ESR measurements, recently published by Hill *et al.*, similar line shifts (by up to 0.28 T) and line shape changes were observed.[33] Similarly to

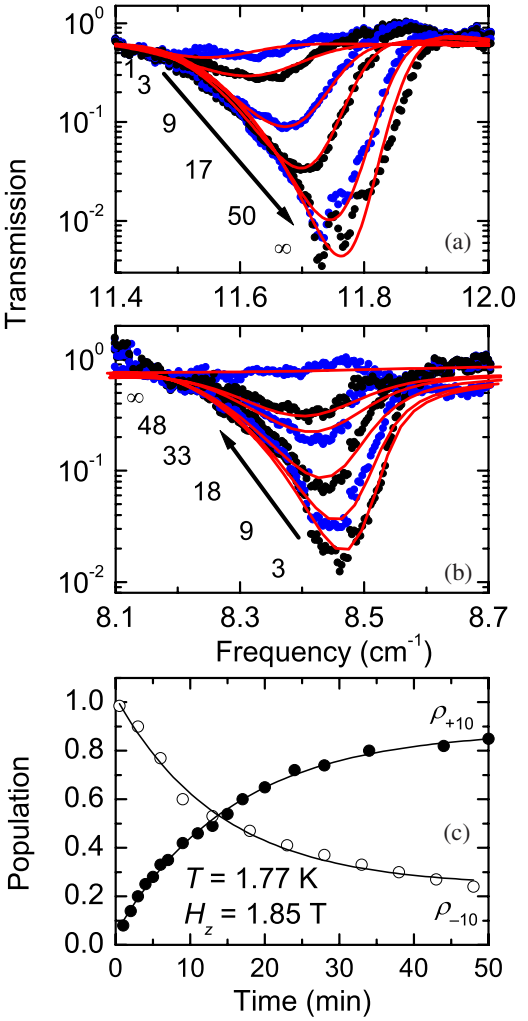

FIG. 5. (Color online) FDMRS spectra recorded on sample V of Mn_{12} at T=1.75 K and various delay times in minutes as indicated. (a) The absorption line corresponding to the $|+10\rangle \rightarrow |+9\rangle$ transition; (b) the resonance line of the $|-10\rangle \rightarrow |-9\rangle$ transition. The solid lines correspond to the calculations from which the population of the respective states can be obtained. (c) Relative populations of the metastable $|-10\rangle$ state (ρ_{-10}, open dots) and the ground $|+10\rangle$ state (ρ_{+10}, full dots).

the measurements presented in this manuscript, the origin of these shifts is presumably also the combined effect of internal dipolar fields and the influence of off-diagonal elements in the magnetic-permeability tensor. The shifts are too large to be explained by internal dipolar fields alone (see below). Quantitative calculation of the effect of these off-diagonal elements on the resonance-line position for cavity measurements is quite challenging.[49]

From fits of the spectra [solid lines in Figs. 5(a) and 5(b), see Sec. III] the populations ρ_{-10} and ρ_{+10} of metastable states and ground states can be extracted, as displayed in Fig. 5(c) as a function of time elapsed after field reversal. The time-dependent populations can be well described by a single exponential decay, and no stretched exponential function is needed. These fits give the time constant $\tau_{-10} = (835 \pm 82)$ s for the depopulation of the metastable state, and $\tau_{+10} = (944 \pm 50)$ s for the increasing population of the

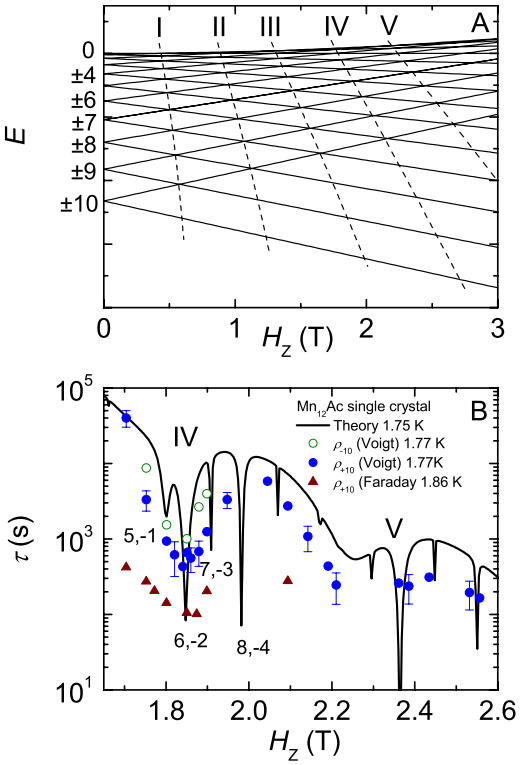

FIG. 6. (Color online) Dependence of the relaxation time on the longitudinal magnetic field. The data are extracted from Voigt geometry measurements ($T=1.77$ K) of the resonance line due to the transition from the metastable state to the ground state (open green circles) and due to the transition from the ground state to the metastable state (closed blue circles). In addition data from measurement in Faraday geometry at 1.86 K are plotted (brown triangles) obtained for fits of the absorption line due to the transition from the ground state to the metastable state. The solid line represents the calculated relaxation time from the phonon-assisted spin tunneling combined with the thermal activation process.

ground state, which are the same within experimental error. These relaxation times in quite reasonable agreement with calculated values (see below). They are longer than those observed by ESR, but the difference in measurement temperature and field precludes more quantitative comparison.

The experiments were repeated at many different applied fields; the extracted relaxation times are displayed Fig. 6). Most importantly, the relaxation time does not show a monotonic dependence on the external magnetic field but exhibits distinct minima at $H_z=+1.85$ T (labeled by IV) and $H_z\approx +2.3$ T (labeled by V); we attribute these to quantum tunneling of the magnetization. Around the second of these minima, the relaxation time is too fast to be measured accurately since inversion of the field takes about 3 min. In the following, we consider the first minimum around 1.85 T in more detail. Without external field, the $\pm M_S$ levels are degenerate. As a function of H_z, periodically levels on the left and right of the energy barrier come into resonance, or, in other words, cross. At these crossings, the transverse terms in the Hamiltonian cause the eigenstates of the system to mix, leading to symmetric and antisymmetric superpositions of the two M_S states involved. The energy difference between those eigenstates is called the tunnel splitting and determines the tunnel rate. The fourth crossing occurs at around $H_z=+1.85$ T. In the absence of fourth-order axial ZFS [i.e., $B=0$ in Eq. (1)], all the different M_S levels would come into resonance at the same H_z, however due to the finite B the individual crossing fields are slightly split. Magnetization relaxation can occur by thermal relaxation, where phonon induced transitions cause the system to ascend to higher and higher lying M_S states until reaching the top of the barrier and descending on the other side. This leads to an Arrhenius type of behavior $\tau=\tau_0 \exp(U/k_BT)$, where U is the energy difference between the metastable and highest-energy M_S state, which is a function of H_z. In the field range studied here, the highest-energy M_S state is $|2\rangle$ for $H_z<2.31$ T, and $|3\rangle$ for larger fields. At the level crossings, the magnetization can also relax by quantum tunneling; its rate depends on the tunnel splitting given by the transverse terms in the Hamiltonian. Because the tunnel splitting of the superposition state that involves $|-10\rangle$ is negligible, quantum tunneling in Mn_{12} occurs always between excited M_S states, a process called thermally activated tunneling (see above). By solving the master equation for the density matrix (see Sec. III and Refs. 53 and 54) which takes into account all possible relaxation paths in the ground multiplet, the total relaxation time can be obtained (Fig. 6). In these calculations a misalignment angle between field and crystal c axis of 2.5° was assumed, to simulate existing internal transverse fields responsible for the tunneling between odd states. This angle demonstrates that the alignment within the sample is not perfect (see Sec. II). The calculated and observed minima match quite well. The experimental relaxation times are slightly shorter than those calculated which may be due to the sample being at a slightly higher temperature than the sensor indicated because it is constantly irradiated. Note that the fine structure that is calculated due to the different individual level crossings is not found in the measurement. This we attribute to the distribution of alignment angles of the different individual crystals in the mosaic of the sample (see Sec. II). In other words, the relaxation is dominated by transverse components of the applied magnetic field due to the misalignment of crystals in the sample, rather than by individual tunneling transitions.

As we noted above, the positions of the resonance lines shift during the experiment. The low-frequency absorption ($|-10\rangle \rightarrow |-9\rangle$) moves to lower frequency, while the transition $|+10\rangle \rightarrow |+9\rangle$ shifts to higher energies. We can calculate the difference of the resonance-line positions due to the transition from the ground state: $\Delta\nu_{+10}=\Delta\nu^{\infty}_{+10}-\Delta\nu^{0}_{+10}$; in Fig. 7(c) this frequency shift is plotted as a function of applied longitudinal field. We observe a distinct minimum at the level-crossing field of approximately 1.85 T. Two interesting observations can be made. First, the shift is larger for the magnetic-resonance transition from the $\Delta\nu_{+10}$ ground state than for the transition from the metastable $\Delta\nu_{-10}$ state. Second, the frequency shift is larger for magnetic fields further away from the level-crossing field [Fig. 7(a)] than close to the level crossing [Fig. 7(b)]. We propose the following qualitative explanation, in which three effects play a role, namely, the internal dipolar field, the line shift due to the nonzero off-diagonal elements in the magnetic-permeability tensor, and the distribution of D-parameter values in the

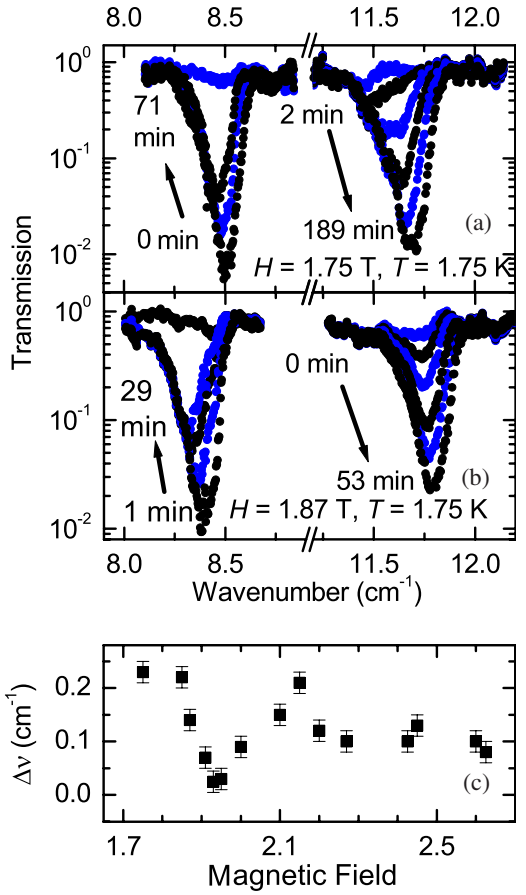

FIG. 7. (Color online) FDMRS spectra recorded on sample V of Mn_{12} at $T=1.75$ K and various delay times. The data in panel A are recorded at $H=1.80$ T, the data in panel B at $H=1.93$ T. Note, that for clarity reasons only a few of the recorded spectra are displayed here. Panel C gives the frequency shift of the resonance line between the first recorded and last recorded spectra for the $|+10\rangle \rightarrow |+9\rangle$ transition as a function of longitudinal magnetic field.

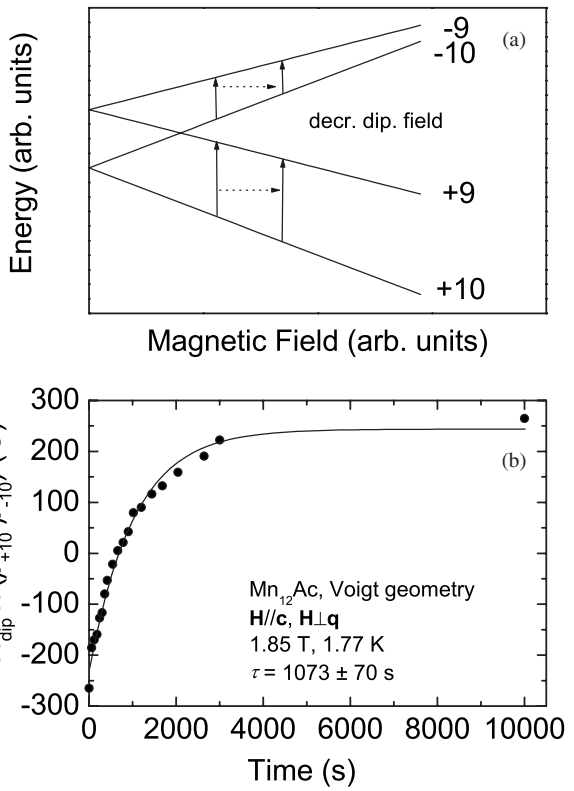

FIG. 8. (a) With increasing internal dipolar field the energy difference of the $|-9\rangle$ and $|-10\rangle$ states decreases, while the transition frequency of the $|+10\rangle \rightarrow |+9\rangle$ increases. (b) Time-dependent local dipolar field $H_{\mathrm{dip}}(\rho_{+10}-\rho_{-10})$ plotted as a function of time. The experimental data belongs to the measurement at $H=1.85$ T, $T=1.77$ K (see text).

sample (D strain). The main cause for the observed line shifts is the change in internal dipolar field during the magnetization relaxation. When the sample is cooled in a magnetic field, the magnetic moments of all molecules are aligned parallel to the external field, and the internal dipolar field adds to the externally applied field. However, after inversion, the internal dipolar field is opposite to the externally applied magnetic field, which means that over time the effective magnetic field increases. The result is that ν_{+10} increases with time, while ν_{-10} decreases [Fig. 8(a)], which is exactly what we have observed, and which was found in INS measurements.[30] From previous studies we found $H_{dip}=26.5$ mT in the fully magnetized state, which is the value we have used in our simulations.[36] From fits of the spectra we extracted the change in dipolar field over time and plot the results in Fig. 8(b). From INS measurements a larger value for $H_{dip}=70$ mT was extracted.[30] Very recently, a value of $H_{dip}=51.5$ mT was reported.[64] There are two effects which cause the magnetic-resonance line due to transitions from both the metastable and ground states to shift to higher frequencies. The first of these two effects is the nonzero off-diagonal elements in the magnetic-permeability tensor. This effect shifts the magnetic-resonance lines from $\nu^0_{\pm 10}$ to $\nu^0_{\pm 10}\sqrt{1+\Delta\mu}$ as discussed above.[36] The second of these two effects is the D strain. Molecules with larger D values have higher energy barriers and will therefore relax more slowly. This implies that the average D value of the populations of both ground and metastable states will increase with time, leading to an increase in resonance frequency, again for both resonance lines. For the transition from the metastable ν_{-10} state those two effects will counteract the effect from the internal dipolar field, and decrease the overall frequency shift. In contrast, for the transition from the ground state (ν_{+10}) all three effects enhance each other, leading to a large frequency shift. This explains that the frequency shift of the magnetic-resonance line during the relaxation of the magnetization is larger for the magnetic-resonance transition from the $\Delta\nu_{+10}$ ground state than for the transition from the metastable $\Delta\nu_{-10}$ state. That leaves the explanation of the second observation, namely, that the frequency shift is larger for magnetic fields further away from the level-crossing field than close to the level crossing. For that we have to note that at the crossing field, the relaxation is to a large extent governed by quantum tunneling of the magnetization. Only those molecules tunnel for which the additional effects of the external field—i.e., the D value and the internal dipolar field—are such that the molecule is exactly at the level crossing. This means that shift in resonance frequency does not nec-

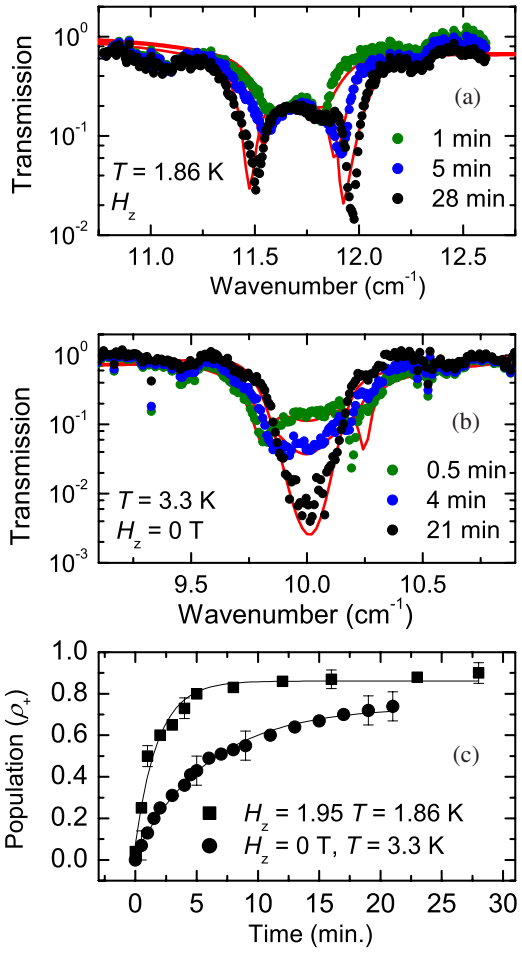

FIG. 9. (Color online) FDMRS transmission spectra recorded on sample F at various delay times as indicated. (a) The data were taken at $T=1.86$ K and $H_z=1.95$ T, and (b) $T=3.3$ K and $H_z=0$ T. (c) Population of the $|+10\rangle$ ground state as a function of time for the measurements in the upper panels.

essarily reflect a certain trend, and concurrently the observed shift in resonance frequency is only small.

C. Relaxation measurements in Faraday geometry

If the external magnetic field is parallel to the direction of radiation propagation we can record spectra in Faraday geometry: $\mathbf{H}\|\mathbf{c}\|\mathbf{q}$. If sample F is cooled down in magnetic field (magnetized state), and the polarizer and analyzer [Fig. 1(a)] are aligned parallel, resonance lines are observed with the characteristic two minima.[39] The plane of radiation polarization experiences a Faraday rotation, and the two minima in transmission correspond to a 90° rotation. Spectra recorded on nonmagnetized crystals show normal resonance lines.[39] This allows us to study magnetization relaxation in Faraday geometry, both in magnetic field and in zero field. Figure 9(a) exhibits an example (at $H=1.85$ T) of spectra recorded over time after inversion of the field, using the same procedure as for the Voigt geometry measurements. The observed resonance lines are due to the $|+10\rangle \rightarrow |+9\rangle$ transition, where the $|+10\rangle$ ground state is gradually populated over time, leading to in increase in sample magnetization and concurrent more pronounced minima in the absorption line. From the fits of the spectra (solid lines), the population of the ground state as a function of time can be extracted [Fig. 9(c)], and from the monoexponential fit the relaxation time is obtained ($\tau=120$ s). If experiment and analysis are repeated at many different fields H_z, we obtain the field-dependence of the magnetization relaxation time (Fig. 6). Note that these experiments were performed at slightly higher temperatures than those in Voigt geometry, and hence the absolute relaxation times are shorter. As in the Voigt measurements, a minimum in the relaxation time is observed, which has shifted to slightly higher fields because of the demagnetizing field. More interestingly, in Faraday geometry we can also study the magnetization relaxation without applying a magnetic field. If the sample is cooled down in a magnetic field, which is then switched off, in order to record FDMRS spectra in zero field, the same double minimum is observed in the magnetic-resonance line shape. Over time, the resonance line gradually assumes a conventional Gaussian line shape in agreement with the fact that the net magnetization of the sample disappears [Fig. 9(b)]. From the population as a function of time [Fig. 9(c)], the relaxation time was determined to be $\tau=350$ s. This result is in particular interesting because it proves that in FDMRS we can perform zero-field relaxation measurements, which is not possible with current cavity or single-pass transmission EPR setups.

V. CONCLUSIONS

We have shown that FDMRS is an excellent method to spectroscopically study magnetization relaxation in single-molecule magnets. Because in FDMRS frequency and magnetic field are independently adjustable, we were able to obtain detailed information on the magnetization relaxation process that could not be obtained with other electron magnetic-resonance methods. The comprehensive investigations on Mn_{12}Ac single crystals in Voigt and Faraday geometry enable the determination of the magnetization relaxation rates, and the clear observation of quantum tunneling of the magnetization. Because magnetic-resonance techniques probe the populations of individual M_S states, we were able to observe the influence of D strain and internal dipolar fields on the resonance-line position. Due to sensitivity limitations of the technique, we were forced to use mosaics of about 20 single crystals rather than one single crystal. This led to a distribution in orientation of the individual crystals which has smeared out some of the fine features that might have been expected in the field dependence of the magnetization relaxation rate.

ACKNOWLEDGMENTS

We thank the Stuttgart Crystal Laboratory for the synthesis of the Mn_{12}Ac crystals. We are especially grateful to Gabriele Untereiner for the skillful assembly of the single-crystal mosaics. We acknowledge the financial support of the Deutsche Forschungsgemeinschaft (DFG) and of the Russian Foundation for Basic Research, Grant No. 07-02-12009-ofi.

*joris.van.slagerен@nottingham.ac.uk

[1] D. Gatteschi, R. Sessoli, and J. Villain, *Molecular Nanomagnets* (Oxford University Press, Oxford, 2006).

[2] D. Gatteschi and R. Sessoli, Angew. Chem. Int. Ed. **42**, 268 (2003).

[3] J. R. Friedman, M. P. Sarachik, J. Tejada, and R. Ziolo, Phys. Rev. Lett. **76**, 3830 (1996).

[4] L. Thomas, F. Lionti, R. Ballou, D. Gatteschi, R. Sessoli, and B. Barbara, Nature (London) **383**, 145 (1996).

[5] W. Wernsdorfer and R. Sessoli, Science **284**, 133 (1999).

[6] A. Ardavan, O. Rival, J. J. L. Morton, S. J. Blundell, A. M. Tyryshkin, G. A. Timco, and R. E. P. Winpenny, Phys. Rev. Lett. **98**, 057201 (2007).

[7] S. Bertaina, S. Gambarelli, T. Mitra, B. Tsukerblat, A. Müller, and B. Barbara, Nature (London) **453**, 203 (2008).

[8] C. Schlegel, J. van Slageren, M. Manoli, E. K. Brechin, and M. Dressel, Phys. Rev. Lett. **101**, 147203 (2008).

[9] H. Miyasaka, R. Clérac, W. Wernsdorfer, L. Lecren, C. Bonhomme, K. Sugiura, and M. Yamashita, Angew. Chem. Int. Ed. **43**, 2117 (2004).

[10] A. J. Tasiopoulos, A. Vinslava, W. Wernsdorfer, K. A. Abboud, and G. Christou, Angew. Chem. Int. Ed. **116**, 2169 (2004).

[11] T. Lis, Acta Crystallogr., Sect. B: Struct. Crystallogr. Cryst. Chem. **36**, 2042 (1980).

[12] S. Carretta, E. Liviotti, N. Magnani, P. Santini, and G. Amoretti, Phys. Rev. Lett. **92**, 207205 (2004).

[13] A. Wilson, J. Lawrence, E. C. Yang, M. Nakano, D. N. Hendrickson, and S. Hill, Phys. Rev. B **74**, 140403(R) (2006).

[14] N. Kirchner, J. van Slageren, B. Tsukerblat, O. Waldmann, and M. Dressel, Phys. Rev. B **78**, 094426 (2008).

[15] S. Carretta, T. Guidi, P. Santini, G. Amoretti, O. Pieper, B. Lake, J. van Slageren, F. El Hallak, W. Wernsdorfer, H. Mutka, M. Russina, C. J. Milios, and E. K. Brechin, Phys. Rev. Lett. **100**, 157203 (2008).

[16] A.-L. Barra, A. Caneschi, A. Cornia, D. Gatteschi, L. Gorini, L. P. Heiniger, R. Sessoli, and L. Sorace, J. Am. Chem. Soc. **129**, 10754 (2007).

[17] A. Cornia, R. Sessoli, L. Sorace, D. Gatteschi, A.-L. Barra, and C. Daiguebonne, Phys. Rev. Lett. **89**, 257201 (2002).

[18] E. del Barco, A. D. Kent, S. Hill, J. M. North, N. S. Dalal, E. M. Rumberger, D. N. Hendrickson, N. Chakov, and G. Christou, J. Low Temp. Phys. **140**, 119 (2005).

[19] W. Wernsdorfer, M. Murugesu, and G. Christou, Phys. Rev. Lett. **96**, 057208 (2006).

[20] S. Takahashi, R. S. Edwards, J. M. North, S. Hill, and N. S. Dalal, Phys. Rev. B **70**, 094429 (2004).

[21] F. Luis, J. Bartolome, and J. F. Fernandez, Phys. Rev. B **57**, 505 (1998).

[22] H. De Raedt, S. Miyashita, K. Michielsen, and M. Machida, Phys. Rev. B **70**, 064401 (2004).

[23] J. M. Hernández, X. X. Zhang, F. Luis, J. Bartolomé, J. Tejada, and R. Ziolo, Europhys. Lett. **35**, 301 (1996).

[24] A. D. Kent, Y. Zhong, L. Bokacheva, D. Ruiz, D. N. Hendrickson, and M. P. Sarachik, Europhys. Lett. **49**, 521 (2000).

[25] I. Chiorescu, R. Giraud, A. G. M. Jansen, A. Caneschi, and B. Barbara, Phys. Rev. Lett. **85**, 4807 (2000).

[26] L. Bokacheva, A. D. Kent, and M. A. Walters, Phys. Rev. Lett. **85**, 4803 (2000).

[27] K. M. Mertes, Y. Suzuki, M. P. Sarachik, Y. Paltiel, H. Shtrikman, E. Zeldov, E. Rumberger, D. N. Hendrickson, and G. Christou, Phys. Rev. Lett. **87**, 227205 (2001).

[28] E. del Barco, A. D. Kent, E. M. Rumberger, D. N. Hendrickson, and G. Christou, Phys. Rev. Lett. **91**, 047203 (2003).

[29] A. Morello, O. N. Bakharev, H. B. Brom, R. Sessoli, and L. J. de Jongh, Phys. Rev. Lett. **93**, 197202 (2004).

[30] O. Waldmann, G. Carver, C. Dobe, D. Biner, A. Sieber, H.-U. Güdel, H. Mutka, J. Ollivier, and N. E. Chakov, Appl. Phys. Lett. **88**, 042507 (2006).

[31] K. Park, M. A. Novotny, N. S. Dalal, S. Hill, and P. A. Rikvold, Phys. Rev. B **66**, 144409 (2002).

[32] S. Hill, R. S. Edwards, S. I. Jones, N. S. Dalal, and J. M. North, Phys. Rev. Lett. **90**, 217204 (2003).

[33] J. Lawrence, S. Lee, S. Kim, S. Hill, M. Murugesu, and G. Christou, AIP Conf. Proc. **850**, 1133 (2006).

[34] J. van Slageren, S. Vongtragool, B. Gorshunov, A. A. Mukhin, N. Karl, J. Krzystek, J. Telser, A. Müller, C. Sangregorio, D. Gatteschi, and M. Dressel, Phys. Chem. Chem. Phys. **5**, 3837 (2003).

[35] M. Dressel, B. Gorshunov, K. Rajagopal, S. Vongtragool, and A. A. Mukhin, Phys. Rev. B **67**, 060405(R) (2003).

[36] S. Vongtragool, A. Mukhin, B. Gorshunov, and M. Dressel, Phys. Rev. B **69**, 104410 (2004).

[37] A. Sieber, C. Boskovic, R. Bircher, O. Waldmann, S. T. Ochsenbein, G. Chaboussant, H.-U. Güdel, N. Kirchner, J. van Slageren, W. Wernsdorfer, A. Neels, H. Stoeckli-Evans, S. Janssen, F. Juranyi, and H. Mutka, Inorg. Chem. **44**, 4315 (2005).

[38] S. Piligkos, G. Rajaraman, M. Soler, N. Kirchner, J. van Slageren, R. Bircher, S. Parsons, H.-U. Güdel, J. Kortus, W. Wernsdorfer, G. Christou, and E. K. Brechin, J. Am. Chem. Soc. **127**, 5572 (2005).

[39] J. van Slageren, S. Vongtragool, A. Mukhin, B. Gorshunov, and M. Dressel, Phys. Rev. B **72**, 020401(R) (2005).

[40] F. El Hallak, J. van Slageren, J. Gómez-Segura, D. Ruiz-Molina, and M. Dressel, Phys. Rev. B **75**, 104403 (2007).

[41] L. Thomas, A. Caneschi, and B. Barbara, Phys. Rev. Lett. **83**, 2398 (1999).

[42] N. Domingo, B. E. Williamson, J. Gomez-Segura, P. Gerbier, D. Ruiz-Molina, D. B. Amabilino, J. Veciana, and J. Tejada, Phys. Rev. B **69**, 052405 (2004).

[43] N. V. Prokof'ev and P. C. E. Stamp, J. Low Temp. Phys. **104**, 143 (1996).

[44] N. V. Prokof'ev and P. C. E. Stamp, Phys. Rev. Lett. **80**, 5794 (1998).

[45] S. Mair, B. Gompf, and M. Dressel, Appl. Phys. Lett. **84**, 1219 (2004).

[46] G. V. Kozlov and A. A. Volkov, Top. Appl. Phys. **74**, 51 (1998).

[47] N. Kirchner, J. van Slageren, and M. Dressel, Inorg. Chim. Acta **360**, 3813 (2007).

[48] M. Dressel and G. Grüner, *Electrodynamics of Solids* (Cambridge University Press, Cambridge, England, 2002).

[49] B. Lax and K. J. Button, *Microwave Ferrites and Ferrimagnetics* (McGraw-Hill Book Company, Inc., New York, 1962).

[50] A. Abragam and B. Bleany, *Electron Paramagnetic Resonance of Transition Ions* (Dover Publications, Inc., New York, 1986).

[51] D. A. Garanin and E. M. Chudnovsky, Phys. Rev. B **56**, 11102 (1997).

[52] A. Fort, A. Rettori, J. Villain, D. Gatteschi, and R. Sessoli, Phys. Rev. Lett. **80**, 612 (1998).

[53] M. N. Leuenberger and D. Loss, Phys. Rev. B **61**, 1286 (2000).

[54] T. Pohjola and H. Schoeller, Phys. Rev. B **62**, 15026 (2000).

[55] A. A. Mukhin, V. D. Travkin, A. K. Zvezdin, S. Lebedev, A. Caneschi, and D. Gatteschi, Europhys. Lett. **44**, 778 (1998).
[56] A. Mukhin, B. Gorshunov, M. Dressel, C. Sangregorio, and D. Gatteschi, Phys. Rev. B **63**, 214411 (2001).
[57] A. B. Sushkov, B. R. Jones, J. L. Musfeldt, Y. J. Wang, R. M. Achey, and N. S. Dalal, Phys. Rev. B **63**, 214408 (2001).
[58] M. Hennion, L. A. Pardi, I. Mirebeau, E. Suard, R. Sessoli, and A. Caneschi, Phys. Rev. B **56**, 8819 (1997).
[59] G. Chaboussant, A. Sieber, S. Ochsenbein, H.-U. Güdel, M. Murrie, A. Honecker, N. Fukushima, and B. Normand, Phys. Rev. B **70**, 104422 (2004).
[60] K. Petukhov, S. Hill, N. E. Chakov, K. A. Abboud, and G. Christou, Phys. Rev. B **70**, 054426 (2004).
[61] A. L. Barra, D. Gatteschi, and R. Sessoli, Phys. Rev. B **56**, 8192 (1997).
[62] S. Hill, J. A. A. J. Perenboom, N. S. Dalal, T. Hathaway, T. Stalcup, and J. S. Brooks, Phys. Rev. Lett. **80**, 2453 (1998).
[63] K. Park, M. A. Novotny, N. S. Dalal, S. Hill, and P. A. Rikvold, Phys. Rev. B **65**, 014426 (2001).
[64] S. McHugh, R. Jaafar, M. P. Sarachik, Y. Myasoedov, H. Shtrikman, E. Zeldov, R. Bagai, and G. Christou, Phys. Rev. B **79**, 052404 (2009).